Physical Drivers and Biogeochemical Effects of the Projected Decline of the Shelfbreak Jet in the Northwest North Atlantic Ocean

Lina Garcia-Suarez[1], Katja Fennel[1], Jasmin G. John[2,3]

[1]Department of Oceanography, Dalhousie University, Halifax, Nova Scotia, Canada

[2]NOAA/OAR/Atlantic Oceanographic and Meteorological Laboratory, Miami, FL

[3]NOAA/OAR/Geophysical Fluid Dynamics Laboratory, Princeton, NJ

Corresponding author: Lina Garcia-Suarez (lina.garcia@dal.ca)

Key Points:

- Temperature-based Gulf Stream North Wall index should not be used in climate future projections.
- Changes in the strength of the southwestward-flowing shelfbreak jet are related to a reduction of the along-shelf pressure gradient.
- Simulated decline in nutrient availability is associated with reduced flow of the nutrient-rich shelfbreak jet.

Abstract

A solid understanding of the mechanisms behind the presently observed, rapid warming of the northwest North Atlantic Continental Shelf is lacking. We hypothesize that a weakening of the Labrador Current System (LCS), especially the shelfbreak jet along the Scotian Shelf, is contributing to these changes and that the future evolution of the LCS will be key to accurate projections. Here we analyze the response of a transient simulation of the high-resolution GFDL Climate Model 2.6 (CM2.6) which realistically simulates the regional circulation but includes only a highly simplified representation of ocean biogeochemistry. Then, we dynamically downscale CM2.6 using a medium-complexity regional biogeochemical ocean model to obtain projections of several ecosystem-relevant variables. In the simulation, the shelfbreak jet weakens throughout the century because of a reduction of the along-shelf pressure gradient caused by a buoyancy gain of the upper water column along the shelf edge. This buoyancy gain is the result of an increased presence of subtropical waters in the continental slope. Importantly, we find that the weakening of the shelfbreak jet is not in response to a northward shift of the Gulf Steam, as has been hypothesized by others, and that previous reports of a northward shift of the Gulf Stream North Wall (GSNW) are an artifact of the temperature-based GSNW criterion in common use. The projected weakening of the shelfbreak jet is likely to lead to a reduction in nutrient availability and a subsequent decline in productivity on the Scotian Shelf, Gulf of St. Lawrence, and Grand Banks.

Plain Language Summary

This paper discusses how global warming affects ocean circulation and biogeochemistry in the northwest North Atlantic. Specifically, we analyze the output of a global climate model that accurately reproduces the trajectory of the Gulf Stream and downscale this model to a regional ocean model to obtain a more detailed biogeochemical response than the climate model provides. We find that changes in the strength of the southwestward-flowing shelfbreak jet are related to changes in the density of the upper slope water and not a northward shift in the core of the Gulf Stream path, as has been postulated by others before us. We show that the simulated decline in nutrient availability on the continental shelf in the northwest North Atlantic is associated with reduced flow of the nutrient-rich shelfbreak jet and a shift towards more nutrient-poor subtropical waters on the shelf. Overall, the findings of this study show the importance of the southwestern branch of the Labrador Current (i.e., the shelfbreak jet) in modulating temporal and spatial variability of shelf waters, making the region particularly vulnerable to climate change impacts.

1 Introduction

The northwest North Atlantic Ocean is a dynamic region particularly sensitive to climate variability due to its position near the confluence of the subtropical and subpolar circulation (Lotze et al., 2022). In this region, cold, fresh waters from the north (Labrador Current) converge with warm, salty Gulf Stream waters from the south (Figure 1). The Labrador Current originates in the Labrador Sea and most of the current flows southward along the northeast Newfoundland Shelf and around the Grand Banks, generally centered near the shelf break (Fratantoni & Pickart, 2007; Loder et al., 1998). At the Tail of the Grand Banks (TGB), the current undergoes a bifurcation, due to the sharp bend in topography, where a branch retroflects towards the northeast

inshore of the North Atlantic Current (Loder et al., 1998) while another continues to follow bathymetry contours as the shelfbreak jet along the shelf edge of the Scotian Shelf, the Gulf of Maine, and the Mid-Atlantic Bight (Chapman & Beardsley, 1989; Fratantoni et al., 2001; Rutherford & Fennel, 2018). The influence of cold, fresh waters from the Labrador Current can be detected as far south as Cape Hatteras (Mertz et al., 1993), where the Gulf Stream separates from the shelf edge (Chi et al., 2019). The relative strength of the two Labrador Current branches is thought to be controlled by the strength of the Labrador Current upstream of the bifurcation and by the position of the Gulf Stream (Jutras et al., 2023).

The shelfbreak jet separates relatively cold, fresh shelf water from warm, salty water over the continental slope, playing a critical role for the transfer of mass and suspended and dissolved materials onto and off the shelf (Flagg et al., 2006; Rutherford & Fennel, 2018). A major, centennial-scale change in the circulation of the Labrador Current is likely underway in response to rising atmospheric carbon dioxide (CO_2) levels (Claret et al., 2018; Gonçalves Neto et al., 2023; Han et al., 2019) and a significant reduction in its along-shelf transport is projected by the end of the 21st century (Rutherford et al., 2023), but the possible impacts of this phenomenon on biogeochemical properties in the region are uncertain.

On the continental shelf in the northwest North Atlantic Ocean, biogeochemical properties such as nutrient, oxygen, and dissolved inorganic carbon (DIC) concentrations are strongly influenced by the subpolar waters of the North Atlantic which are rich in DIC, oxygen, and nutrients (Petrie & Yeats, 2000; Rutherford & Fennel, 2022). Thus, a central question is how the changes in ocean circulation would affect nutrient availability and primary production on the northwest North Atlantic shelf under a climate scenario where the transport of the Labrador Current and shelfbreak jet decline. Conventional approaches to addressing this question involve multi-model ensemble averages from Earth System Models (ESM) or dynamical downscaling of global climate projections from ESMs or climate models with regional circulation models that better simulate shelf processes and dynamics (Holt et al., 2009). ESMs however, have generally coarse model grids which do not adequately represent the bathymetry and circulation of shelf areas in the northwest North Atlantic (Fennel et al., 2022). The Coupled Model Intercomparison Project Phase 5 – CMIP5 (Taylor et al., 2012) and Phase 6 – CMIP6 (Eyring et al., 2016) ensemble of ESMs have a warm bias in sea surface temperature due to a misrepresentation of the Gulf Stream position (Moreno-Chamarro et al., 2021; Saba et al., 2016) and poor performance on simulating surface nitrate and chlorophyll in the region (Laurent et al., 2021), compromising their ability to depict causes and effects of climate change in the coastal ocean between Cape Hatteras and the Tail of the Grand Banks. While representation of the northwest North Atlantic regional circulation can be improved by increasing the ocean model horizontal resolution (Saba et al., 2016), increasing the grid resolution of global ESMs is computationally prohibitive at this time (Stock et al., 2011). We therefore decided to analyze the response of a high-resolution climate model to increasing atmospheric carbon dioxide concentrations and dynamically downscale it to a regional ocean circulation model coupled with a biogeochemical model to improve the complex process representation on the shelves.

The objective of this study is to explore the potential drivers and effects of the weakening of the Labrador Current on nutrient availability and primary production along the northwest North Atlantic shelf by analyzing a high-resolution climate model and downscaling it to a regional ocean-biogeochemical coupled model. First, we used an Empirical Orthogonal Function (EOF) analysis to determine the role of anthropogenic climate change on large scale variability

of seawater temperature and salinity in the climate model. Second, we investigated whether the weakening of the shelfbreak jet is related to a northward shift in the Gulf Stream path, as well as the relationship between the increased presence of subtropical waters in the upper water column of the continental slope and the physical processes driving the long-term decrease in volume transport of the shelfbreak jet. Finally, we analyzed the downscaled changes in ecosystem-relevant variables: nitrate, chlorophyll, salinity, and temperature on the Scotian Shelf and present plausible mechanisms associated with those changes.

2 Materials and Methods

2.1 Climate Model

We used the output from the Geophysical Fluid Dynamics Laboratory (GFDL) climate model CM2.6 (Delworth et al., 2012) to investigate the long-term variability of physical ocean properties (section 3.1) and the driver of the projected weakening of the shelfbreak jet (section 3.2) on the northwest Atlantic Ocean. CM2.6 is a high-resolution coupled atmosphere-ocean-land-sea ice global model that includes a reduced-complexity ocean biogeochemical model. The atmospheric circulation model has an average spatial resolution of 0.5° x 0.5° (50 km) and the ocean component has a horizontal resolution of 0.1° x 0.1° (10 km) and 50 vertical layers (see Figure 1 for the section of the CM2.6 domain used in this study). The biogeochemical model (miniBLING) consists of three state variables: dissolved inorganic carbon (DIC), phosphate (PO_4), and oxygen (Galbraith & Martiny, 2015). After a spin-up phase of 120 years at the constant preindustrial level of atmospheric CO_2 (286 ppm), two simulations were performed for an additional 80 years: a control scenario in which atmospheric CO_2 was held constant at 286 ppm, and a warming scenario in which atmospheric CO_2 increased by 1% per year over 70 years until it doubled, and then remained at this level for 10 additional years. Details of the two simulations can be found in Delworth et al. (2012).

The rapid increase of CO_2 in the warming scenario can be scaled to resemble the increase of CO_2 in the RCP6 scenario (Moss et al., 2010) through a relationship described in Claret et al. (2018). Since the atmospheric CO_2 increases faster in the CM2.6 experiment than in the RCP6 scenario, this scaling stretches the modeled time series so its time axis roughly corresponds to the historical and future RCP6 CO_2 trajectory. We note that the simulation represents an idealized case with increasing of CO_2 only and does not account for other forced climate changes due to atmospheric aerosols, non-CO_2 GHGs, and ozone.

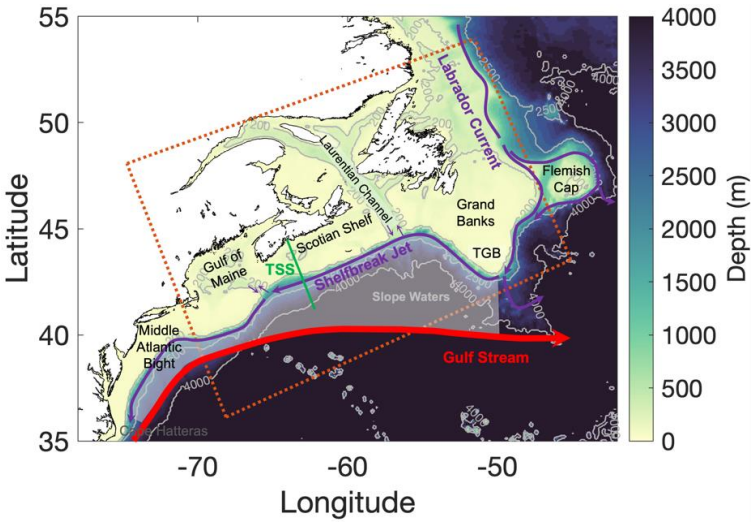

Figure 1. Schematic of the large-scale circulation in the Northwest Atlantic Ocean, the CM2.6 bathymetry, and some geographical features. The map shows the section of the CM2.6 domain used to force the regional Atlantic Canada Model (ACM). The orange dotted line indicates the boundary of the regional model grid. Purple arrows are colder, fresher waters associated with the Labrador Current. The red arrow represents the warm, salty Gulf Stream. The green line shows a transect (TSS) across the Scotian Shelf and part of the slope water region (white shading between shelfbreak jet and Gulf Stream arrows).

2.2 EOF analysis method

We performed an empirical orthogonal function (EOF) analysis (Preisendorfer (1988), Korres et al. 2000) to assess the dominant spatial patterns/modes and temporal variability in the temperature and salinity fields of the CM2.6 warming simulation (section 3.1). Let us assume a time series of de-seasoned 3D fields (i.e., temperature or salinity) denoted by the column vector $\phi(r_i, t)$ where r_i is the 3D position vector $r_i = (x_i, y_i, z_i)$ that determines the position of the ith grid point at the time t. The EOF procedure expresses the dataset as a modal expansion:

$$\phi(r_i, t) \approx \sum_{n=1}^{N} a_n(t)\psi_n(r_i) \qquad 1)$$

where a_n are the temporal evolution functions (principal component or PC scores) and $\psi_n(r_i)$ the spatial eigenfunctions (EOF) or modes. The modes ψ_n are the eigenvectors of the covariance matrix of $\phi(r_i, t)$ while the eigenvalues measure the mean squared projection of the data onto the nth empirical eigenfunction or, in other words, the amount of variance explained by each EOF. Assuming the terms in (1) are arranged in descending order of the corresponding eigenvalues, a few leading terms generally provide good estimates of the ocean fields. We sought the physical interpretation of the leading EOF modes and their relationship with long-term changes in ocean circulation due to atmospheric CO_2 increase, hence we eliminated the seasonal cycle from each time series before performing the EOF analysis by subtracting the calculated monthly mean climatology at each grid cell. The climatology was calculated from the full 80-year period of the detrended CM2.6 warming simulation. Since long-term local changes in

temperature and salinity were found to be nonlinear, we chose to keep the local trend and thus the response to climate change in the EOF analysis.

2.3 Regional biogeochemical model

We use the Atlantic Canada Model (ACM), a coupled physical-biogeochemical configuration of the Regional Ocean Modeling System, ROMS v3.5 (Haidvogel et al., 2008), to downscale the biogeochemical projections from the CM2.6 warming scenario (section 3.3). The ACM has 30 topography-following vertical levels, a horizontal grid spacing of ~10 km on the shelf, and covers the northwest North Atlantic with the same domain and physics described in Brennan et al., (2016). The domain includes the Gulf of Maine, Scotian Shelf, Grand Banks, and East Newfoundland Shelf (Figure 1). Rutherford and Fennel (2018) have shown that the model realistically represents present-day circulation patterns. The biogeochemical model is based on the nitrogen-cycle model of Fennel et al. (2006) with expansions by Fennel et at. (2008) to include the inorganic carbon component and by Laurent et al. (2021) to include two size classes each for phytoplankton, chlorophyll, zooplankton, and detritus. Laurent et al. (2021) and Rutherford et al. (2021) have shown that the model represents the present-day biological seasonality realistically. The ACM was run here for 101 years from 1999 to 2100. In the first 7 years some of the biogeochemical variables (i.e., dissolved oxygen and DIC) drifted, hence those years were considered model spin-up and not used in the analysis. Only outputs from the years 2006 to 2100 were used. Daily 3D averages of physical and biogeochemical properties were saved.

2.4 Dynamical downscaling method

We dynamically downscaled the CM2.6 projection by using a time-varying delta method to obtain initial and boundary conditions, including the surface atmospheric fluxes, for the regional ACM. We first interpolated ocean, atmospheric, and biogeochemical variables from CM2.6 to the regional model grid using objective analysis. Then, we calculated time-varying deltas by subtracting the CM2.6 monthly climatology (warming scenario; model years 1-80) from the entire simulation period (i.e., years 1-80) at each grid cell. The time dimension of these time-varying deltas was then transformed so that the doubling trajectory of atmospheric CO_2 closely resembles that of the RCP6 scenario between 1999 and 2100, following Claret et al. (2018) and Rutherford et al. (2023). In the case of physical ocean variables (i.e., temperature, salinity, velocity, and sea surface height), the stretched time-varying deltas were added to the monthly, present-day climatology (1999–2004) from Urrego-Blanco & Sheng (2012). The time-varying deltas for the biogeochemical variables (DIC, dissolved oxygen, and PO_4) were calculated annually, because the CM2.6 biogeochemical outputs are available only as annual means, and then added to the present-day, monthly biogeochemical climatology defined in Kuhn and Fennel (2019) and Rutherford et al. (2021). This monthly climatology is based the World Ocean Atlas 2009 (Garcia et al., 2010) and relationships with temperature and salinity determined from bottle data for the region. For atmospheric forcing variables (i.e., shortwave and longwave radiation, air temperature, pressure, humidity, precipitation, and winds), stretched time-varying deltas were added to a present-day baseline made up of a 3-hourly time series from 1999 to 2016 from the European Centre for Medium-range Weather Forecasts' (ECMWF) global

atmospheric reanalysis ERA-Interim (Dee et al., 2011) and repeated (~6 times) to cover the entire period of interest.

The reconstructed ocean variables and atmospheric forcing retain the observed historical climatology and high-frequency variability while inheriting the long-term change and interannual variability projected in the CM2.6 warming scenario. Pozo-Buil et al. (2021) showed that this time-varying delta method is advantageous over the "fixed delta" method frequently used in climate studies (Alexander et al., 2020; Shin & Alexander, 2020) because it can capture projected changes in interannual variability and resolve potentially non-linear impacts of climate change that would be missed if the transient response were excluded with the "fixed delta" method. Biological conditions for nitrate, DIC, and dissolved oxygen needed an additional treatment since the CM2.6 biogeochemical model output is only available between 2065 and 2100 in both control and warming scenarios as 3D annual means. Firstly, we converted CM2.6 PO_4 output to nitrate (NO_3) using the Redfield ratio. Next, we calculated the deltas at each grid cell, as described above, and then we averaged over the available period to get one biological delta. Then, we assumed a linear increase from delta = 0 in the year 1999, when the regional biogeochemical model was initialized, to the calculated mean delta at the end of the century.

3 Results

3.1 Long -term seawater temperature and salinity variability under a warming scenario

We used the warming scenario of the CM2.6 model, which has been found to show a more realistic simulation of the Gulf Stream relative to coarser model versions (Caesar et al., 2018; Saba et al., 2016), to investigate the role of anthropogenic CO_2 in driving long-term changes of temperature and salinity in the northwest North Atlantic Ocean. The leading EOF of the de-seasoned temperature anomalies shows a warming signal over nearly the entire domain, representing 57.9 % of the overall variability (Figure 2). The temporal pattern associated with the first mode is characterized by an increasing trend between 2010 and 2048, a peak around 2050 followed by a downward trend until 2060, and steady increase thereafter (Figure 2f). The spatial pattern of the first EOF shows enhanced warming at the subsurface (around 200 m depth), downstream of the TGB and along the continental shelf break and slope (Figure 2 b, e). At and below 750 m, the warming of Slope waters is negligible (Figure 2 c, d).

The first EOF of de-seasoned salinity anomalies shows a similar temporal pattern as the first temperature EOF, with an increasing trend from 2010 to 2043 and after 2064, and peak around 2050 (Figure 3f). The spatial pattern is characterized by a dipole trend with freshening (negative EOF values) of the upper ocean in the northern half of the domain (north of ~ 42 °N; Figure 3a), and salinification (positive EOF values) in both the south and at mid-depths around 200 m, downstream of the TGB and into the Laurentian Channel (Figure 3 b, e). At 750 m and below, the signal is negligible along the Slope (Figure 3 c, d). Salinification is prominent along the continental slope between Cape Hatteras and Georges Bank at the surface (Figure 3a) and further offshore the Scotian Shelf at around 100 m depth (Figure 3e).

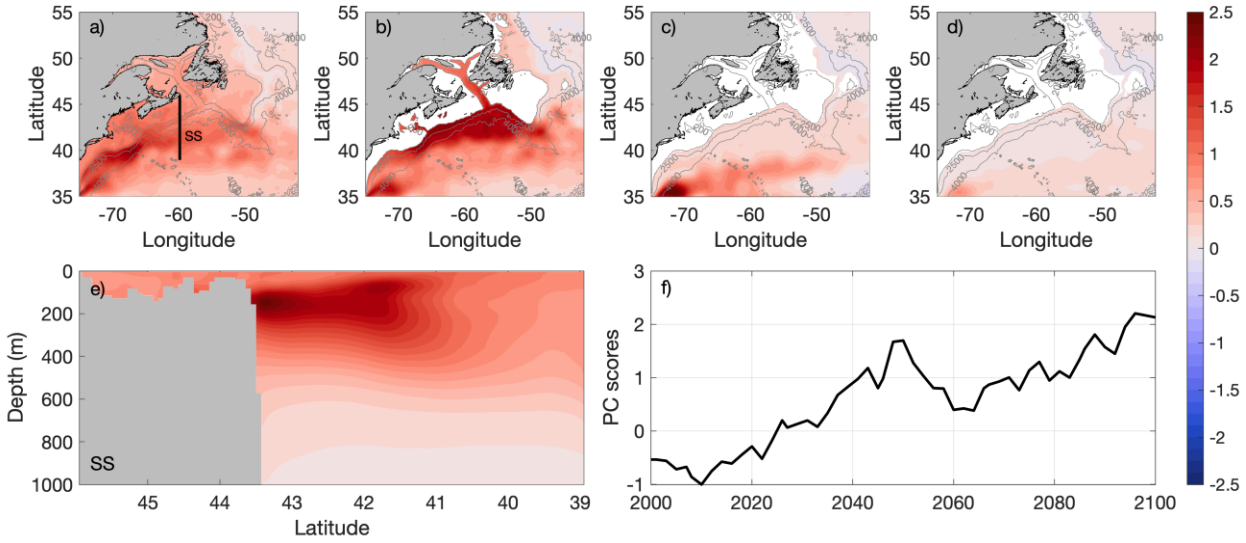

Figure 2. Leading EOF of de-seasoned temperature in the CM2.6 warming case at surface (a), 200 m (b), 750 m (c), 1000 m (d), along SS transect (e; transect shown in panel (a)), and PC scores (f). First EOF explains 57.9 % of the total variance. The second EOF explains 4.6 % of the total variance (not shown).

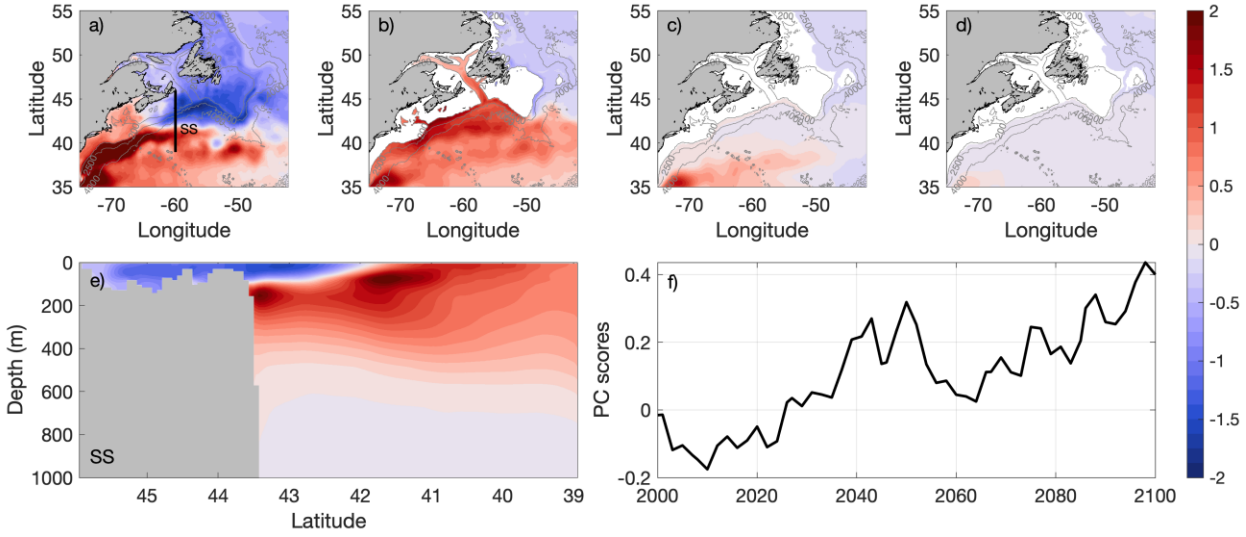

Figure 3. Leading EOF of salinity in the CM2.6 warming case at surface (a), 200 m (b), 750 m (c), 1000 m (d), along SS transect (e), and PC scores (f). First EOF explains 45.1 % of the total variance. Second EOF explains 6.0 % of the total variance (not shown).

A change in salinity and temperature causes a change in the density profile and thus the vertical stratification. We use potential energy anomaly (PEA), a measure for the amount of work required to fully mix the water column (Simpson, J, 1981), to analyze the projected changes in stratification in the Northwest North Atlantic Ocean under the CM2.6 warming scenario. Supplementary Figure S1 shows the mean spatial distribution of PEA over water depth (PEA/H) in the upper ocean (surface to 200 m depth) and the projected changes in the 21st

century. We show PEA/H instead of PEA, as PEA increases with increasing water depth H, which would give weaker weight to shallower shelf areas.

The highest values of PEA/H are found along the shelf break in the slope area and in the Laurentian Channel. With the intensified sea surface warming and freshening projected by the model, most of the shelf regions will experience an increase in stratification. The change in the vertical structure of salinity enhances the stratification along the shelf break and slope area. These areas are susceptible to surface freshening and increased temperature and salinity at depth (Figure 2 and Figure 3) strongly altering the vertical structure of density. Stations located in the Scotian Shelf (SS), Laurentian Channel Mouth (LCM), and Grand Banks (GB) shelf break, and depicted in Supplementary Figure S1, demonstrate the enhanced stratification between 2040 and 2050, as well as by the end of the century similar to the pattern observed in the leading EOF modes of variability (Figure 2 and Figure 3), whereas stations in the central Gulf of Maine (GoM) and East Newfoundland Shelf (ENS) show negative or near-zero changes in PEA. Stratification is also strengthened close to Cape Hatteras, probably as a consequence of the increased presence of salty subtropical water, and weakened in the subtropical gyre along the Gulf Stream and the shelf break downstream of the Scotian Shelf.

3.2 Projected shelfbreak jet weakening and its physical driver

The warm, salty Gulf Stream water is separated from the cold, fresh shelf water by the slope water. There is a sharp temperature front in the limit between the Gulf Stream and the slope water known as the Gulf Stream North Wall (GSNW) which is usually represented by the 15°C isotherm at 200 m depth (Joyce et al., 2000). The trajectory of the GSNW has been referred to as the position of the Gulf Stream in many studies (Caesar et al., 2018; Peterson et al., 2017; Seidov et al., 2019). Figure 4 shows that the maximum surface current speed, associated with the Gulf Stream core, and the GSNW are close to each other only to the west of 65°W (around Cape Hatteras), but rapidly decouple farther east even under pre-industrial conditions (Supplementary Figure S2).

Use of the maximum surface velocity as a proxy for the Gulf Stream path has the disadvantage that the maximum velocity of the strongly meandering free jet becomes disjointed past Cape Hatteras due to the existence of meanders and eddies, especially between 70°W and 60°W (Figure 4). Eddies can have comparable, and sometimes even larger, surface velocities than the Gulf Stream main axis, resulting in physical jumps in the Gulf Stream position. However, large-scale surface circulation is known to roughly follow sea surface height (SSH) contours (Häkkinen, 2001), and several studies have approximated the Gulf Stream path along the 0.25-m SSH contour line from altimetry data which coincides with the location of the velocity maximum (Andres, 2016; Lillibridge & Mariano, 2013). The specific SSH contour associated with the Gulf Stream path in a numerical model may differ from that in observations because SSH in models typically refers to a different geoid than altimetry data. In this study, we use the -0.23-m SSH as a proxy for the simulated mean Gulf Stream path, which corresponds with most of the surface maximum velocity points, even east of 70°W, in both warming and control scenarios (Figure 4 and Supplementary Figure S2).

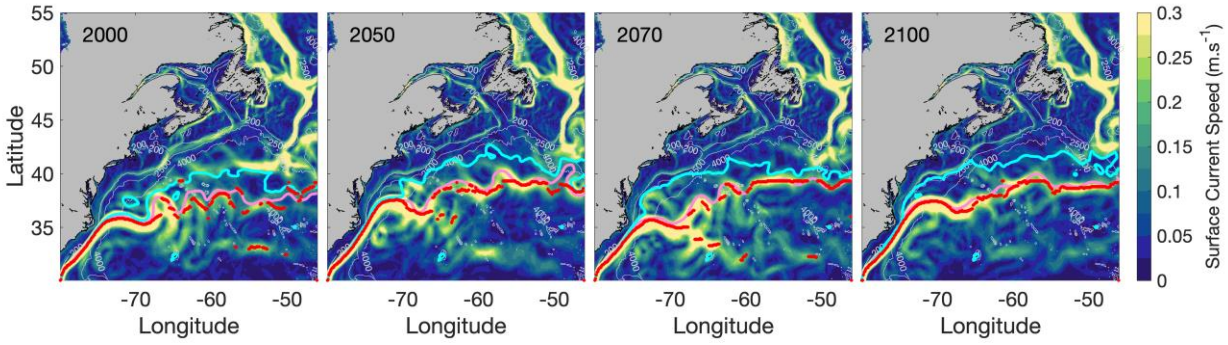

Figure 4. Annual surface current speed over years 2000, 2050, 2070, 2100 in the CM2.6 warming scenario (color scale). The cyan line indicates the mean GSNW (15°C isotherm at 200 m depth). The pink line indicates the Gulf Stream path (-0.23 m SSH contour). The maximum surface velocity at each longitude is represented by the red points. Gray contours show the 200m, 2500m, and 4000m isobaths.

Figure 5 depicts the annual mean position of both the GSNW and the Gulf Stream path in the warming and control scenarios of the CM2.6, from 2000 to 2100. The mean GSNW and Gulf Stream path in the control scenario separates from the US east coast at Cape Hatteras and turns east below 40°N to continue its journey through the North Atlantic Ocean (Figure 5a, d). In contrast, the warming scenario exhibits a greater amplitude in the GSNW position and after the mid 21st century it becomes attached to the shelf edge between Cape Hatteras and Georges Banks closer to the TGB (Figure 5b). However, this northward shift is not observed in the main path of the Gulf Stream core which mainly maintains a similar position in both warming and control scenarios (Figure 5d, e).

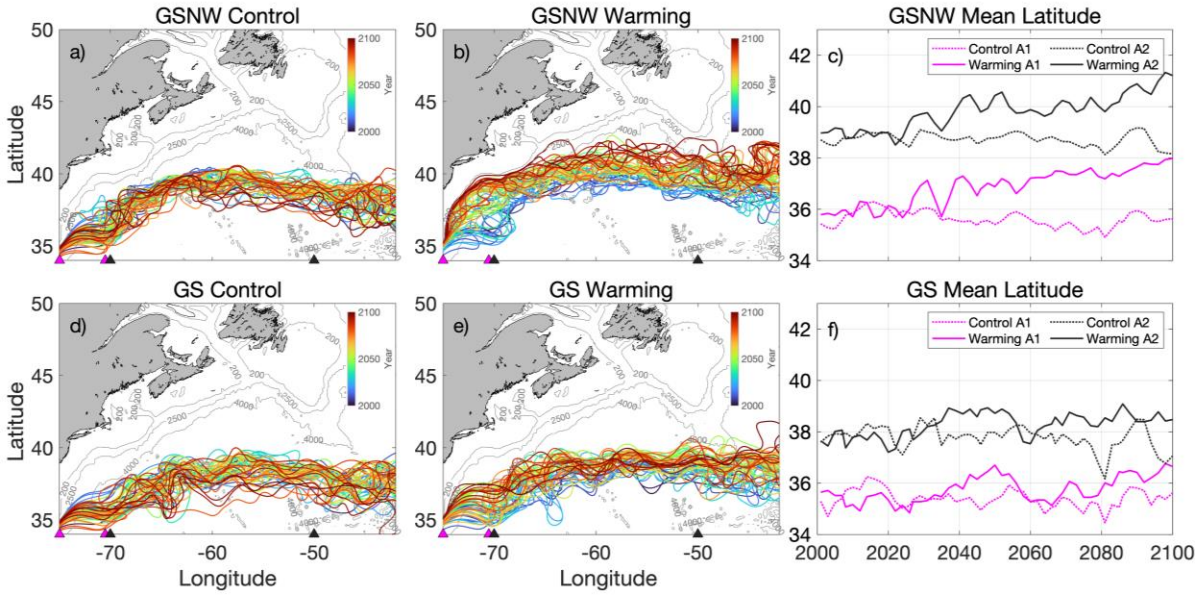

Figure 5. Position of the annually averaged GSNW (15°C isotherm at 200 m depth) for each year from 2000 to 2100 in the CM2.6 control (a) and warming scenarios (b). Annual mean latitude of the GSNW (c) estimated by averaging latitudes of each trajectory in two regions: region A1 (75°W to 71°W) delimited by the pink triangles and the mean latitude represented

with pink lines, and region A2 (70°W and 50°W) delimited by the black triangles and the mean latitude is represented with black lines. Dotted lines show the mean latitude in the control scenario and continuous lines show the mean latitude in the warming scenario. Panels (d), (e), and (f) show the same features as in panels (a), (b), and (c), respectively but for the Gulf Stream (GS) path (-0.23 m SSH contour).

To determine how far north the GSNW migrates compared to the Gulf Stream path, the mean latitude of both indices are evaluated in two subregions: one close to Cape Hatteras between 75°W and 71°W (region A1 in Figure 5) where the Gulf Stream separates from the continental margin, and in the region between 70°W and 50°W (region A2 in Figure 5) in the slope sea. Under a warming scenario, a northward shift in the GSNW is observed in both regions (Figure 5c), clearly differentiated from its preindustrial (control) trend after 2037. In terms of the Gulf Stream path, there might be a slight northward move in region A1 after 2060 but it is not distinguishable from the natural variability in the preindustrial scenario (Figure 5f).

In the warming projection, subtropical waters impinge on the slope between Cape Hatteras and the TGB, increasing temperature and salinity in the upper 300 m of the water column and widening the separation between the GSNW and the path of the Gulf Stream (Supplementary Figure S3to S5). The increased presence of warm, salty water on the slope results in an increase the sea surface height (SSH) inshore of the 4000-m isobath with consequences for the continuity of the Labrador Current west of the Grand Banks, i.e., the shelfbreak current. Future projections of density, current speed, and SSH in the CM2.6 warming scenario compared to present-day conditions are shown in Figure 6. In a present-day scenario (2000-2020), the shelfbreak jet is steered by the steep topography and driven by pronounced horizontal density gradients (Figure 6a). At the shelf break, the subsurface horizontal density gradient between denser, cooler sub-polar water and warmer, buoyant subtropical water provides a baroclinic contribution to the southwestward along-shelf flow (Figure 6d). In the future scenario (2080-2100), the subsurface density along the continental shelfbreak and slope is strongly reduced, especially downstream of the TGB (Figure 6b, c), essentially leading to a significant reduction of the shelfbreak jet downstream (Figure 6e, f). Changes in the density of the upper water column, along with atmospheric variability, yield a sea level shift at the TGB, hence a decrease of the along-shelf barotropic pressure gradient. Under a high atmospheric CO_2 concentration scenario, a shift toward higher SSH is observed along the shelf break and shoreward of the 4000-m isobath by the end of the century, especially in the area between the Scotian Shelf and the TGB (Figure 6h, i). This pattern coincides with weaker circulation of the shelf break jet west of the Grand Banks.

An important driving force for currents in some regions of the Northwest Atlantic Ocean is the along-shelf pressure gradient (ASPG) (Beardsley & Boicourt, 1981), here represented as the along-shelf SSH gradient. In present-day and future time slices, the sea surface slopes up from north to south along the equatorward flowing shelfbreak jet core (Figure 6j). The linear fits yield slopes between the TGB and SS of $^{\Delta SSH}/_{\Delta x} \approx 1.29x10^{-7}$ in the present-day time slice (blue dotted line in Figure 6j) and a lower slope of $^{\Delta SSH}/_{\Delta x} \approx 6.27x10^{-8}$ in the future -time slice (pink dotted line in Figure 6j), indicating a reduction in the ASPG of around 51% over the 21st century.

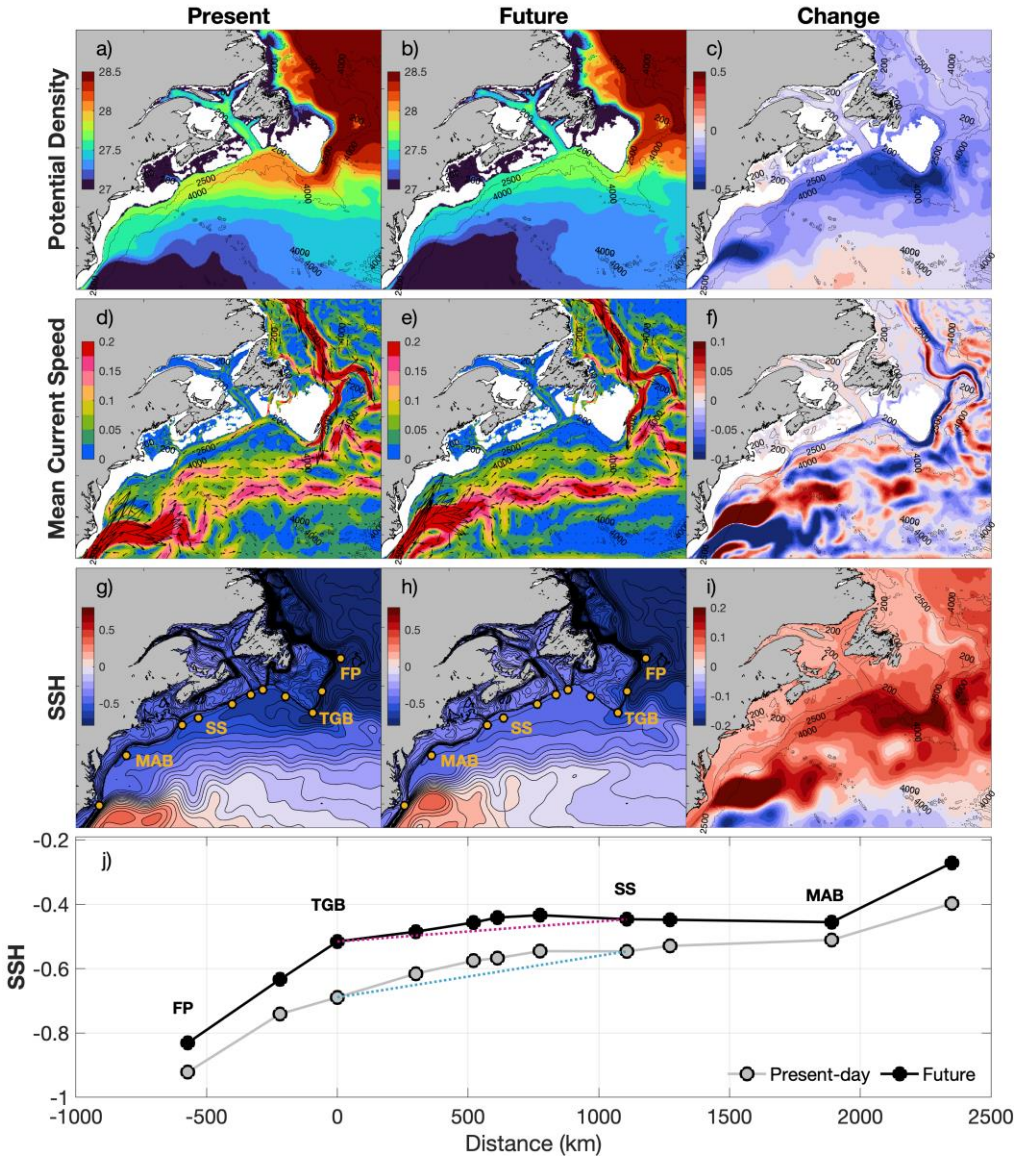

371

372 **Figure 6.** Mean ocean potential density (km.m^{-3}), current speed (m.s^{-1}), and sea surface height
373 (SSH; m) in the Northwest Atlantic in the CM2.6 warming case in a present-day (2000-2020; a,
374 d, g) and future (2080-2100; b, e, h) periods and the change (future minus present; c, f, i). Mean
375 subsurface (100-300 m) potential density (a, b, c) with the 200-m, 2500-m, and 4000-m isobath
376 contoured in black. Mean subsurface (100-300 m) current speed with directions as black arrows
377 (d, e, f). Mean SSH with black contours every 0.01 m on shelves but 0.05 m elsewhere and
378 yellow dots representing the station locations (g, h, i). Mean SSH at stations along the shelf
379 break jet core with distance measured from the Tail of Grand Banks (TGB; j). Indicated locations
380 are Flemish Pass (FP), Scotian Shelf (SS), TGB, and Middle Atlantic Bight (MAB). The dotted
381 lines indicate linear regressions from TGB to SS.
382

383 In order to evaluate the relationship of the ASPG with the continuity of the shelfbreak jet,
384 we plotted the annual mean SSH gradient, the depth evolution of the isopycnal σ_θ = 27.25 kg.m^{-3},
385 and the along-shelf southwestward volume transport on the Scotian Shelf break (Figure 7). Even

manuscript submitted to *Journal of Advances in Though the SSH gradient and volume transport show large fluctuations in Figure 7, they are expected to decrease from around 1.4 x 10^{-7} and 1.7 Sv in the 2000s to 0.6 x 10^{-7} and 0.4 Sv in 2100, respectively; a reduction of ~ 57% in the case of SSH gradient and ~75% for the volume transport. Figure 7 also shows that the isopycnal σ_θ = 27.25 kg.m^{-3} deepens by around 30 m over the century. The along-shelf SSH gradient is anticorrelated with the deepening of the isopycnal σ_θ = 27.25 kg.m^{-3} (correlation coefficient: -0.69), which is strongly correlated with the southward volume transport along the Scotian Shelf break (correlation coefficient: 0.86; right panel in Figure 7). In other words, the rapid decrease in the along-shelf SSH gradient, the buoyancy gain by the upper water column, and the weakening of the shelf-break jet coincide suggesting a causal relation.

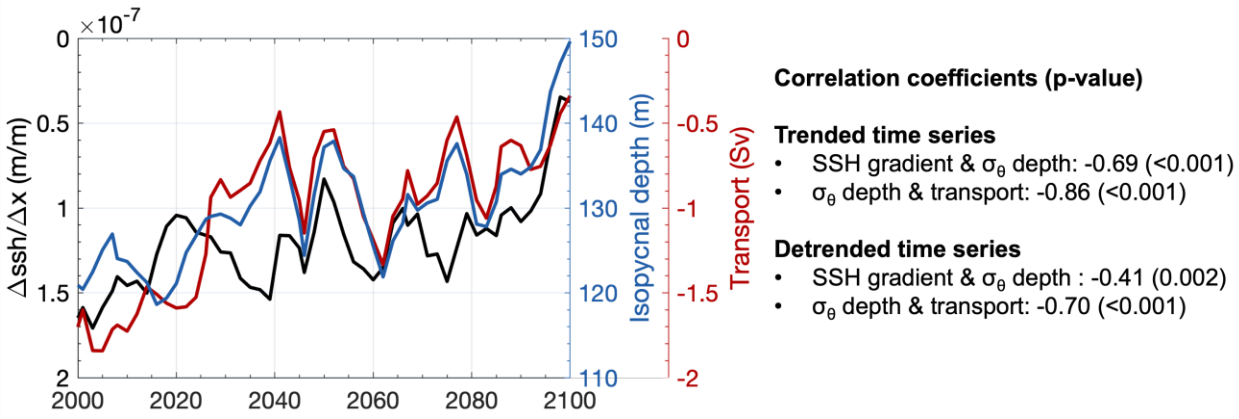

Figure 7. 100-yr time series of annual mean SSH gradient (dimensionless, black line), southwestward volume transport (top to 500 m depth, red line), and depth of the isopycnal σ_θ = 27.25 kg.m^{-3} , (blue line) at station SS in Figure 6. SSH gradient is calculated between station TGB and SS in Figure 6. Sv: Sverdrup. Correlation coefficients between the three variables are shown on the right panel. Note that the left y-axis is reversed for visual improvement. Negative values of volume transport represent southwestward flow.

However, along-shelfbreak volume transport does not decline equally over the water column. Figure 8 suggests a significant decrease in net annual mean volume transport at the TGB and downstream of it, especially for depth bins at or greater than 100 m where the core of the shelfbreak jet is located (Fratantoni & Pickart, 2007). In particular, net transport at 200 m and 500 m declines almost completely after 2027 and by the end of the 21st century at SS and TGB, respectively (Figure 8b, c) and in some years the net mean flow is reversed, with poleward flow dominating. At the eastern Grand Banks (between Flemish Cap and the TGB), changes in net volume transport are negligible over the century (Figure 8a). Therefore, the weakening of the southwestward branch of the Labrador Current (shelfbreak jet) may not be strongly affected by the strength of the Labrador Current before reaching the TGB.

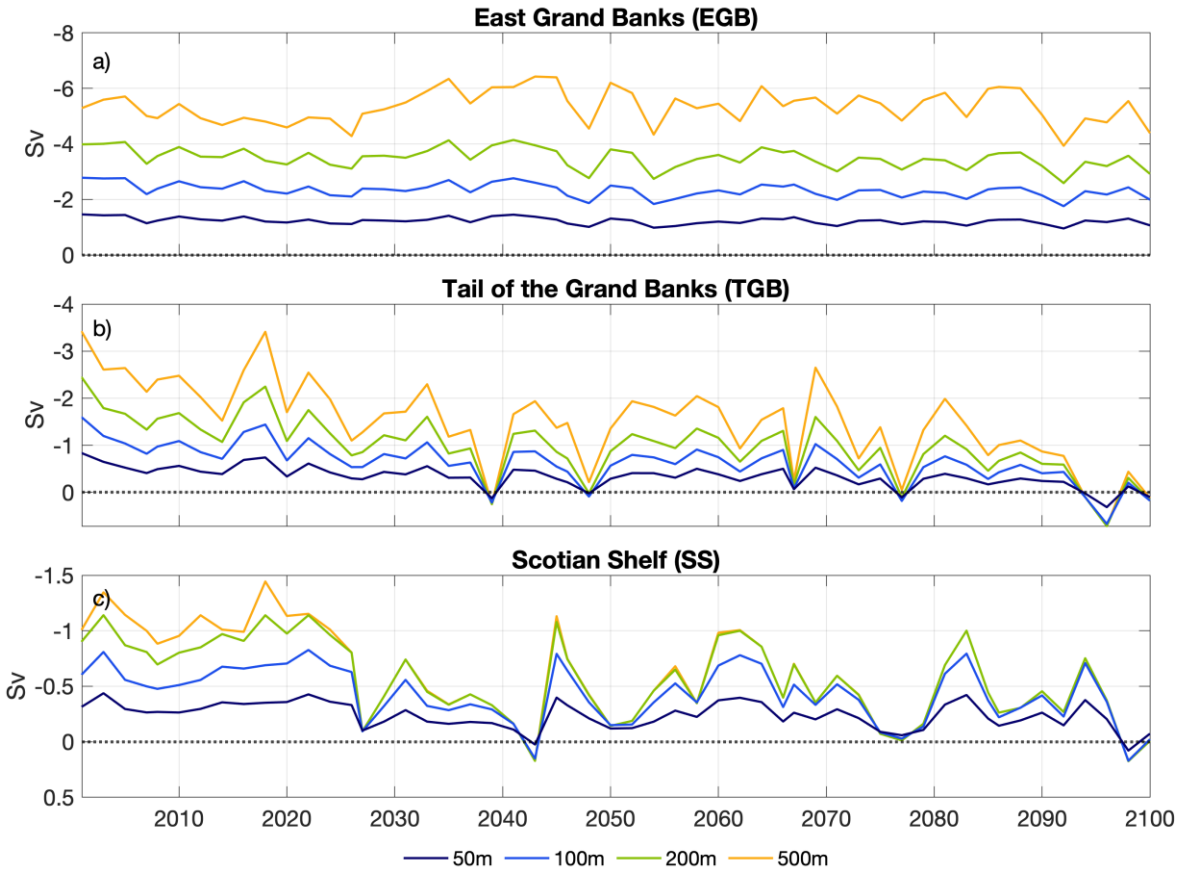

Figure 8. Along-shelf volume transport across three cross-shelf lines in the northwest North Atlantic Ocean. The transect locations are shown in Supplementary Figure S6 Annual mean net volume transport (Sv) in the CM2.6 warming scenario in vertical bins from surface to: 50 m (dark blue line), 100 m (blue line), 200 m (green line), and 500 m (yellow line) across the three transects. Transports are positive for flow in the general northeast direction and negative for transports in the southwest direction. The horizontal black dotted line shows the zero transport x-axis. Net transport: balance between equatorward and poleward transport

3.3 Biogeochemical impacts on the Scotian Shelf

The downscaled response of the circulation shift in the Northwest Atlantic is shown in Figure 9. The increased presence of subtropical waters at the TGB and the reduced transport of the southwestward branch of the Labrador Current make the shelf break and slope area of the Northwest Atlantic Ocean a hotspot of climate change impacts. The upper-ocean (0-200 m depth) temperature is projected to increase over the entire Northwest Atlantic domain, with pronounced changes in temperature and salinity downstream of the TGB and along the shelf break, including the Laurentia Channel mouth, where temperature increases between 3 °C and 4 °C (Figure 9a, e) accompanied by a rise in salinity > 0.3 (Figure 9b, f) due to inflow of slope waters. The effects of meltwater runoff and sea ice reduction in the Labrador Sea, one of the most affected regions by the changing climate in the subpolar North Atlantic (Zhang et al., 2021), and the reduced transport of the shelfbreak jet, have the potential to lead to a freshening of the upper ocean (0 to 200 m depth) on the Grand Banks, parts of the Gulf of St. Lawrence, and

northeastern Scotian Shelf (Figure 9 b, f). A reduction between 1.0 and 2.5 mmol N. m^{-3} in NO_3 concentration (Figure 9 c,g), and between 1.3 and 2.9 mmol N. $m^{-2}.day^{-1}$ in net primary productivity (NPP) (Figure 9 d, h) is also projected in the region, with a prominent drop in NO_3 in the Gulf of St. Lawrence and around the TGB. The mechanisms behind this long-term decline are the subject of further investigation.

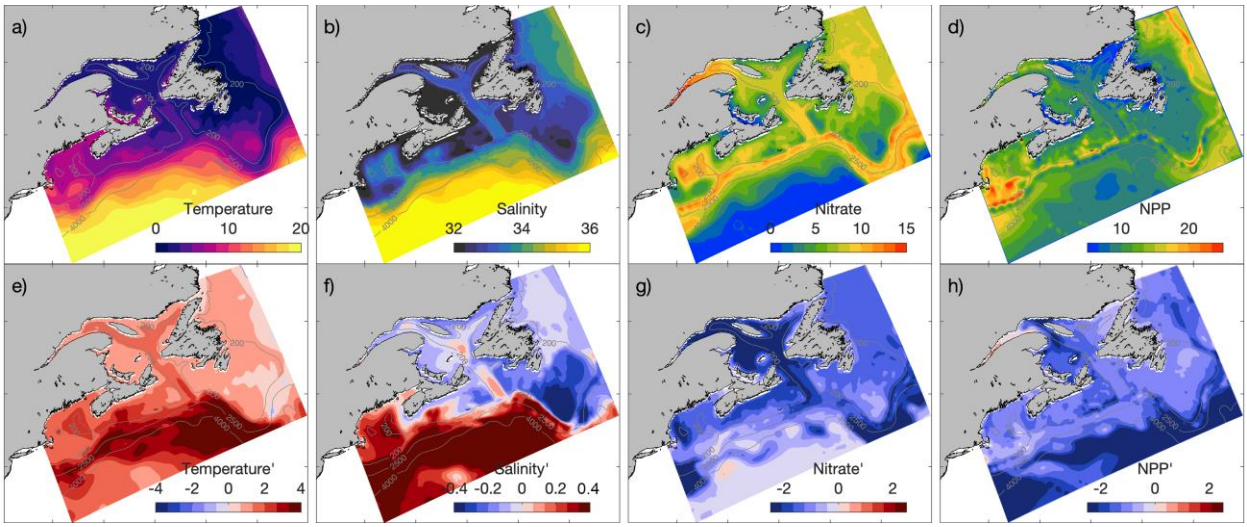

Figure 9. Maps of present-day (2006-2020; top row) and future changes (2080-2100 relative to present-day; bottom row) of depth-averaged (top to 200 m depth) temperature in °C (a, e), salinity (b, f), nitrate (NO_3) in mmol $N.m^{-3}$ (c, g), and vertically integrated net primary productivity (NPP) in mmol $N.m^{-2}.day^{-1}$

On the Scotian Shelf, local changes in physical properties, along with the reduced transport of the water flowing down the Labrador Shelf along the shelf break, will undoubtedly have an impact on the biogeochemistry. The continuous weakening of the southwestward flow of the shelfbreak jet at the edge of the Scotian Shelf (Figure 10a) contributes to a rapid shelf warming by allowing warmer offshore waters to impinge on the shelf (Figure 10b). Maximum southwestward, along-shelf velocity at the core of the shelfbreak jet (black triangle in Figure 10a) varies from -0.09 $m.s^{-1}$ in 2006 to -0.03 $m.s^{-1}$ in 2100, while depth-averaged temperature in the deep basin (red triangle in Figure 10b) increases from 7.7 °C in 2006 to 10.8 °C in 2100. The intrusion of warm slope waters to the Scotian Shelf is reflected in a pronounced decline of depth-averaged nitrate from 6.0 mmol $N.m^{-3}$ in 2006 to 4.7 mmol $N.m^{-3}$ in 2100 at the deepest point of the basin (red triangle in Figure 10c). This reduction leads to a more limited supply of nutrients to phytoplankton and is reflected in a reduction of the subsurface chlorophyll and phytoplankton biomass maximum. At 50 m depth, where the maximum values of chlorophyll and phytoplankton biomass are found (Figure 10d), concentrations decline ~50 % from 0.93 $mg.m^{-3}$ in 2006 to 0.46 $mg.m^{-3}$ in 2100 in terms of chlorophyll, and ~ 34% from 0.85 to 0.56 mmol $N.m^{-3}$ in terms of phytoplankton biomass, at the deep basin (red triangles in Figure 10d, e).

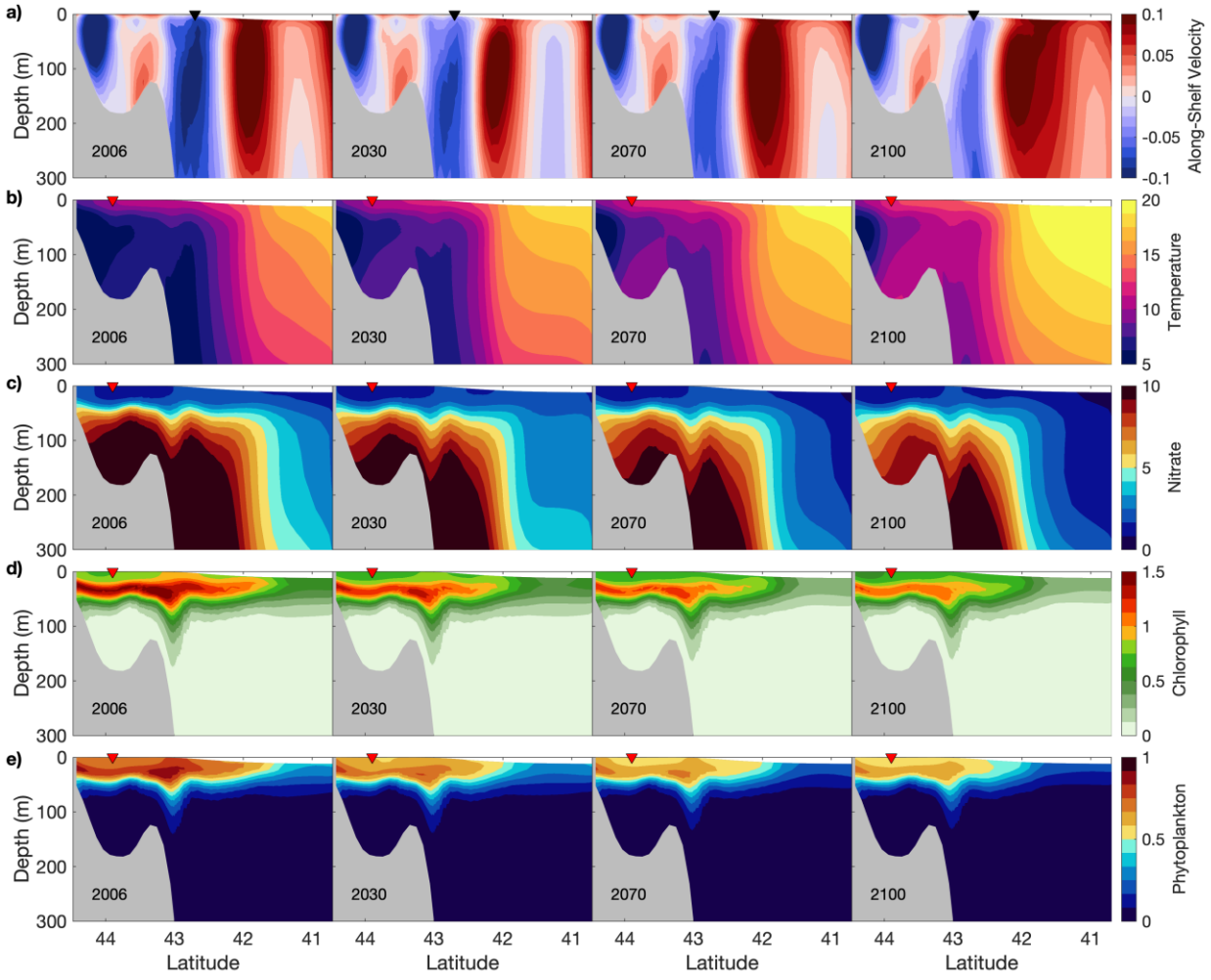

Figure 10 Vertical sections of annual mean in years 2006, 2030, 2070, and 2100 of along-shelf velocity (a), temperature (b), nitrate (c), chlorophyll (d), and phytoplankton biomass (e) along transect TSS in Figure 1. The velocity is normal to the section where blue shades represent equatorward flow and red shades represent poleward flow. Black triangle shows the core of the shelfbreak jet. Red triangles depict the deepest point on the shelf. Linear trends of each variable are shown in Figure S7 in the Supplementary Information

4 Discussion

Our analyses of a CO_2-driven climate change scenario show a projected decline in the volume transport of the Labrador Current past the Grand Banks in the 21st century (Figure 8) and a decrease in nitrate availability to the Gulf of St. Lawrence, the Tail of the Grand Banks (TGB) and intermediate and bottom waters on the Scotian Shelf (Figure 9 and Figure 10). The high-resolution climate model (CM2.6) shows an enhanced warming of the northwest North Atlantic subsurface waters along the shelf break and continental slope between the TGB and the Scotian Shelf (Figure 2). This warming is accompanied by a pronounced surface freshening and a subsurface salinification (Figure 3) caused by an increased presence of subtropical water in the slope (Supplementary Figure S4 and Figure S5). Previous studies have associated the changes in

the upper water column properties with a northerly shift in the Gulf Stream path (Caesar et al., 2018; Gonçalves Neto et al., 2021; Saba et al., 2016; Seidov et al., 2019). Particularly, Caesar et al. (2018) and Seidov et al. (2019) used the variability of the temperature-based GSNW index as marker of the shift in the Gulf Stream trajectory between 75°W and 50°W. However, our results show that the GSNW and the Gulf Stream path are close to each in front of the Middle Atlantic Bight until 70°W but diverge farther east, even under preindustrial atmospheric conditions. Our finding agrees with Chi et al. (2019) who claim that the GSNW is not a good indicator for the position of the Gulf Stream, due to the temperature anomaly introduced by mesoscale eddies that causes a loss of correlation between the movements of the stream and its north wall. We complement their conclusion by saying that this temperature-based index should not be used in climate future projections, east of 70°W, since the separation of the GSNW and Gulf stream widens as the ocean warms. Under a climate change scenario, changes in the slope seawater temperature are prominent due to the increased presence of subtropical water that pushes the warm, salty waters onto the edge of the continental shelf, but it does not imply spatial changes in the core of the Gulf Stream location as the analysis of the surface current speed reveals (Figures 4, 5).

The depth-dependent changes in temperature and salinity alter the density profile and thus the vertical stratification (Supplementary Figure S1). The deepening of the isopycnal σ_θ = 27.25 kg.m^{-3} in Figure 7 reflects the buoyancy gain by the upper water column, due to an increase in buoyant subtropical waters and a reduced presence of the Labrador Current waters in the slope. The rise in vertical stratification along the shelf break and slope area shown here is consistent with the CMIP6 global projections (Kwiatkowski et al., 2020). Yet the reasons behind the reduced stratification in the Slope region between Cape Hatteras and the southern Scotian Shelf are unclear. Density stratification controls the stability of the upper ocean and it can modulate vertical mixing which in turn affects the availability of remineralized nutrients in the upper ocean (Cheng et al., 2013). Therefore, it is possible that the strengthening of stratification in most of the shelf edge is one of the causes of the reduction in the supply of nutrients to the euphotic zone in our downscaled regional model (ACM; Figure 9).

Our results suggest that the changes in the density of the upper water column are correlated with the reduction of the along-shelf pressure gradient (ASPG) that plays an important role in explaining the weakening of the southwestward flowing shelfbreak jet. Stommel and Leetmaa (1972) concluded that an ASPG or sea surface slope of order 10^{-7} (dimensionless) must exist to drive the mean alongshore flow southwestward against the mean wind stress. In this study, the modeled ASPG agrees with that threshold even though we found a reduction of nearly 51% of the ocean surface slope (between TGB and SS) by the end of the 21st century under a future warming scenario compared to present-day conditions. It suggests that ASPG will continue to be a contributor in driving the along-shelf currents even in a climate change scenario. However, the shift of subtropical water masses northwards causes a rapid increase in SSH at the TGB compared to other Northwest Atlantic Ocean locations (see Figure 6g). This shift reduces the along-shelf sea surface slope, hence the ASPG and the southwestward transport of the Labrador Current west of the Grand Banks.

By the end of the 21st century, southwestward along-shelf volume transport is significantly reduced by ~75% compared to present-day values at the Scotian Shelf break. The disruption of Labrador Current flow at the shelf break is so drastic in the 2040's and 2090's that the shelfbreak jet net volume transport is reversed for several years, flowing in a poleward

direction (Figure 8). These changes might be a consequence of enhanced Gulf Stream eddies and meander generation that, as Gonçalves-Neto et al. (2023) suggest, have the potential to impinge on the shelf break along the Grand Banks and block or disrupt the equatorward flow of the Labrador Current.

Nutrients are advected to the northwest North Atlantic Ocean and shelves via the Labrador Current System, specifically the shelfbreak jet (Rutherford & Fennel, 2022), and the runoff of the St. Lawrence River (Petrie & Yeats, 2000). As expected, the downscaled upper-ocean (0 to 200 m depth) nitrate concentrations in the northwest North Atlantic Ocean follow a similar trend of nitrate global depletion (-1.06 ± 0.45 mmol m^{-3}) projected by the ESMs participating in the CMIP6 forced under the high-emission scenario SSP5-8.5 (Kwiatkowski et al., 2020). We noted that nitrate decreases rapidly along the southern edge of the Grand Banks, the Gulf of St. Lawrence, and at shallow depths on the Scotian Shelf and Gulf of Maine (Figure 9c, g). Particularly on the Scotian Shelf, the enhanced stratification and the weak connectivity of the Labrador Current result in a greater reduction in the supply of nutrients to the euphotic zone leading to an enhanced nutrient limitation and declines in the subsurface phytoplankton biomass and chlorophyll maximum (Figure 10).

Our results are consistent with earlier studies by Rutherford & Fennel (2018) and Rutherford et al. (2023). These studies suggested that the shelfbreak jet strength plays a key role in maintaining distinct mid-depth and bottom temperature and salinity as well as biogeochemical properties such as pH and DIC on the shelf by inhibiting ocean-shelf exchange (cross-shelf flux). Once the shelfbreak jet weakens, the influence of warm, salty, nutrient depleted slope water increases on the shelves. The impingement of slope waters is already altering the regional ecosystem (Bianucci et al., 2016) and has likely contributed to long-noted trends in fisheries (Davis et al., 2017; Nye et al., 2009). Already now, increased mortality and a poleward latitudinal shift across species has been found during extreme weather events (Mills et al., 2013; Pershing et al., 2015; Zisserson & Cook, 2017), therefore in a future scenario where atmospheric CO_2 continuously increases and the shelfbreak jet weakens, changes in temperature, salinity, buoyancy, and nutrient availability will likely affect productivity, patterns of species richness and consequential changes in marine goods and services in the Northwest Atlantic shelves even more.

5 Conclusions

The high-resolution projections presented here show that the increasing presence of subtropical waters, instead of a northward shift of the Gulf Stream trajectory, and the reduced transport of the southwestward branch of the Labrador Current make the shelf break and slope area of the northwest Atlantic Ocean particularly vulnerable to climate change impacts. The Labrador Current's flow past the Grand Banks is projected to decline in the 21st century, which is likely to lead to a reduction in nutrient supply and a subsequent decline in productivity of the Scotian Shelf, Gulf of St. Lawrence, and the Grand Banks. The processes determining the supply of nutrients to the shelf including cross-shelf exchange fluxes and the southwestward transport of subpolar waters are simulated realistically in our downscaled model but tend to be missed by typical ESMs due to their coarse spatial resolution.

Overall, the findings of this study contribute to a deeper understanding of the dynamical drivers of the southwestern branch of the Labrador Current (i.e. the shelfbreak jet) and its

importance in modulating temporal and spatial variability of shelf waters. These dynamic connections have important implications for projecting long-term changes in the Northwest North Atlantic Ocean. Even though this case study is based on an idealized scenario where CO_2 increases steadily over most of the 21st century and does not account for other greenhouse gases, the downscaled regional projection provides the physical and biogeochemical foundation for considering impacts on higher trophic levels (e.g., as input to species distribution models). Finally, the results of this study raise new questions about the role of the shelfbreak jet in intra-annual variability of ecosystem-relevant variables (e.g., pH, DIC, dissolved oxygen) under a changing climate and provide testable hypotheses for future work.

Acknowledgments

Elizabeth Drenkard is acknowledged for her comments and suggestions on an internal review of the manuscript.

Open Research

The ROMS code is available at https://www.myroms.org. Annual means of the model output, from year 2000 to 2100, will be available in a DOI repository for the final submission.

References

Alexander, M. A., Shin, S., Scott, J. D., Curchitser, E., & Stock, C. (2020). The Response of the Northwest Atlantic Ocean to Climate Change. Journal of Climate, 33(2), 405–428. https://doi.org/10.1175/JCLI-D-19-0117.1

Andres, M. (2016). On the recent destabilization of the Gulf Stream path downstream of Cape Hatteras. Geophysical Research Letters, 43(18), 9836–9842. https://doi.org/10.1002/2016GL069966

Beardsley, R., & Boicourt, W. (1981). On estuarine and continental-shelf circulation in the Middle Atlantic Bight. In Evolution of Physical Oceanography: Scientific Surveys in Honor of Henry Stommel, B. A. Warren and C. Wunsch. MIT Press. Retrieved from https://ocw.mit.edu/courses/res-12-000-evolution-of-physical-oceanography-spring-2007/6ab42a55551a514396755040a53de529_wunsch_chapter7.pdf

Bianucci, L., Fennel, K., Chabot, D., Shackell, N., & Lavoie, D. (2016). Ocean biogeochemical models as management tools: a case study for Atlantic wolffish and declining oxygen. ICES Journal of Marine Science: Journal Du Conseil, 73(2), 263–274. https://doi.org/10.1093/icesjms/fsv220

Brennan, C., Blanchard, H., & Fennel, K. (2016). Putting Temperature and Oxygen Thresholds of Marine Animals in Context of Environmental Change: A Regional Perspective for the Scotian Shelf and Gulf of St. Lawrence. PLOS ONE, 11(12), e0167411. https://doi.org/10.1371/journal.pone.0167411

Brennan, C. E., Bianucci, L., & Fennel, K. (2016). Sensitivity of Northwest North Atlantic Shelf Circulation to Surface and Boundary Forcing: A Regional Model Assessment. Atmosphere-Ocean, 54(3), 230–247. https://doi.org/10.1080/07055900.2016.1147416

613 Caesar, L., Rahmstorf, S., Robinson, A., Feulner, G., & Saba, V. (2018). Observed fingerprint of
614 a weakening Atlantic Ocean overturning circulation. Nature, 556(7700), 191–196.
615 https://doi.org/10.1038/s41586-018-0006-5

616 Caesar, L., McCarthy, G. D., Thornalley, D. J. R., Cahill, N., & Rahmstorf, S. (2021). Current
617 Atlantic Meridional Overturning Circulation weakest in last millennium. Nature
618 Geoscience, 14(3), 118–120. https://doi.org/10.1038/s41561-021-00699-z

619 Chapman, D. C., & Beardsley, R. C. (1989). On the Origin of Shelf Water in the Middle Atlantic
620 Bight. Journal of Physical Oceanography, 19(3), 384–391. https://doi.org/10.1175/1520-
621 0485(1989)019<0384:OTOOSW>2.0.CO;2

622 Cheng, W., Chiang, J. C. H., & Zhang, D. (2013). Atlantic Meridional Overturning Circulation
623 (AMOC) in CMIP5 Models: RCP and Historical Simulations. Journal of Climate, 26(18),
624 7187–7197. https://doi.org/10.1175/JCLI-D-12-00496.1

625 Chi, L., Wolfe, C. L. P., & Hameed, S. (2019). The Distinction Between the Gulf Stream and Its
626 North Wall. Geophysical Research Letters, 46(15), 8943–8951.
627 https://doi.org/10.1029/2019GL083775

628 Claret, M., Galbraith, E. D., Palter, J. B., Bianchi, D., Fennel, K., Gilbert, D., & Dunne, J. P.
629 (2018). Rapid coastal deoxygenation due to ocean circulation shift in the northwest
630 Atlantic. Nature Climate Change, 8(10), 868–872. https://doi.org/10.1038/s41558-018-
631 0263-1

632 Davis, X. J., Joyce, T. M., & Kwon, Y.-O. (2017). Prediction of silver hake distribution on the
633 Northeast U.S. shelf based on the Gulf Stream path index. Continental Shelf Research,
634 138, 51–64. https://doi.org/10.1016/j.csr.2017.03.003

635 Dee, D. P., Uppala, S. M., Simmons, A. J., Berrisford, P., Poli, P., Kobayashi, S., et al. (2011).
636 The ERA-Interim reanalysis: configuration and performance of the data assimilation
637 system. Quarterly Journal of the Royal Meteorological Society, 137(656), 553–597.
638 https://doi.org/10.1002/qj.828

639 Delworth, T. L., Rosati, A., Anderson, W., Adcroft, A. J., Balaji, V., Benson, R., et al. (2012).
640 Simulated Climate and Climate Change in the GFDL CM2.5 High-Resolution Coupled
641 Climate Model. Journal of Climate, 25(8), 2755–2781. https://doi.org/10.1175/JCLI-D-
642 11-00316.1

643 Eyring, V., Bony, S., Meehl, G. A., Senior, C. A., Stevens, B., Stouffer, R. J., & Taylor, K. E.
644 (2016). Overview of the Coupled Model Intercomparison Project Phase 6 (CMIP6)
645 experimental design and organization. Geoscientific Model Development, 9(5), 1937–
646 1958. https://doi.org/10.5194/gmd-9-1937-2016

647 Fennel, K., Wilkin, J., Levin, J., Moisan, J., O'Reilly, J., & Haidvogel, D. (2006). Nitrogen
648 cycling in the Middle Atlantic Bight: Results from a three-dimensional model and
649 implications for the North Atlantic nitrogen budget: NITROGEN CYCLING IN THE
650 MIDDLE ATLANTIC. Global Biogeochemical Cycles, 20(3), n/a-n/a.
651 https://doi.org/10.1029/2005GB002456

652 Fennel, K., Wilkin, J., Previdi, M., & Najjar, R. (2008). Denitrification effects on air-sea CO 2
653 flux in the coastal ocean: Simulations for the northwest North Atlantic. Geophysical
654 Research Letters, 35(24), L24608. https://doi.org/10.1029/2008GL036147

Fennel, K., Mattern, J. P., Doney, S. C., Bopp, L., Moore, A. M., Wang, B., & Yu, L. (2022). Ocean biogeochemical modelling. Nature Reviews Methods Primers, 2(1), 1–21. https://doi.org/10.1038/s43586-022-00154-2

Flagg, C. N., Dunn, M., Wang, D.-P., Rossby, H. T., & Benway, R. L. (2006). A study of the currents of the outer shelf and upper slope from a decade of shipboard ADCP observations in the Middle Atlantic Bight. Journal of Geophysical Research, 111(C6), C06003. https://doi.org/10.1029/2005JC003116

Fratantoni, P. S., Pickart, R. S., Torres, D. J., & Scotti, A. (2001). Mean Structure and Dynamics of the Shelfbreak Jet in the Middle Atlantic Bight during Fall and Winter*. Journal of Physical Oceanography, 31(8), 2135–2156. https://doi.org/10.1175/1520-0485(2001)031<2135:MSADOT>2.0.CO;2

Fratantoni, Paula S., & Pickart, R. S. (2007). The Western North Atlantic Shelfbreak Current System in Summer. Journal of Physical Oceanography, 37(10), 2509–2533. https://doi.org/10.1175/JPO3123.1

Galbraith, E. D., & Martiny, A. C. (2015). A simple nutrient-dependence mechanism for predicting the stoichiometry of marine ecosystems. Proceedings of the National Academy of Sciences, 112(27), 8199–8204. https://doi.org/10.1073/pnas.1423917112

Garcia, H. E., Locarnini, R. A., Boyer, T. P., Antonov, J. I., Zweng, M. M., Baranova, O. K., & Johnson, D. R. (2010). World Ocean Atlas 2009, Volume 4: Nutrients (phosphate, nitrate, silicate) (NOAA Atlas ednruther, Vol. 4). Washington, D.C.: U.S. Government Printing Office. Retrieved from https://www.ncei.noaa.gov/sites/default/files/2020-04/woa09_vol4_text.pdf

Gonçalves Neto, A., Langan, J. A., & Palter, J. B. (2021). Changes in the Gulf Stream preceded rapid warming of the Northwest Atlantic Shelf. Communications Earth & Environment, 2(1), 74. https://doi.org/10.1038/s43247-021-00143-5

Gonçalves Neto, A., Palter, J. B., Xu, X., & Fratantoni, P. (2023). Temporal Variability of the Labrador Current Pathways Around the Tail of the Grand Banks at Intermediate Depths in a High-Resolution Ocean Circulation Model. Journal of Geophysical Research: Oceans, 128(3). https://doi.org/10.1029/2022JC018756

Haidvogel, D. B., Arango, H., Budgell, W. P., Cornuelle, B. D., Curchitser, E., Di Lorenzo, E., et al. (2008). Ocean forecasting in terrain-following coordinates: Formulation and skill assessment of the Regional Ocean Modeling System. Predicting Weather, Climate and Extreme Events, 227(7), 3595–3624. https://doi.org/10.1016/j.jcp.2007.06.016

Häkkinen, S. (2001). Variability in sea surface height: A qualitative measure for the meridional overturning in the North Atlantic. Journal of Geophysical Research: Oceans, 106(C7), 13837–13848. https://doi.org/10.1029/1999JC000155

Han, G., Ma, Z., Long, Z., Perrie, W., & Chassé, J. (2019). Climate Change on Newfoundland and Labrador Shelves: Results From a Regional Downscaled Ocean and Sea-Ice Model Under an A1B Forcing Scenario 2011–2069. Atmosphere-Ocean, 57(1), 3–17. https://doi.org/10.1080/07055900.2017.1417110

Holt, J., Harle, J., Proctor, R., Michel, S., Ashworth, M., Batstone, C., et al. (2009). Modelling the global coastal ocean. Philosophical Transactions of the Royal Society A:

Mathematical, Physical and Engineering Sciences, 367(1890), 939–951. https://doi.org/10.1098/rsta.2008.0210

Joyce, T. M., Deser, C., & Spall, M. A. (2000). The Relation between Decadal Variability of Subtropical Mode Water and the North Atlantic Oscillation*. Journal of Climate, 13(14), 2550–2569. https://doi.org/10.1175/1520-0442(2000)013<2550:TRBDVO>2.0.CO;2

Jutras, M., Dufour, C. O., Mucci, A., & Talbot, L. C. (2023). Large-scale control of the retroflection of the Labrador Current. Nature Communications, 14(1), 2623. https://doi.org/10.1038/s41467-023-38321-y

Korres, G., Pinardi, N., & Lascaratos, A. (2000). The Ocean Response to Low-Frequency Interannual Atmospheric Variability in the Mediterranean Sea. Part II: Empirical Orthogonal Functions Analysis. Journal of Climate, 13(4), 732–745. https://doi.org/10.1175/1520-0442(2000)013<0732:TORTLF>2.0.CO;2

Kuhn, A. M., & Fennel, K. (2019). Evaluating ecosystem model complexity for the northwest North Atlantic through surrogate-based optimization. Ocean Modelling, 142, 101437. https://doi.org/10.1016/j.ocemod.2019.101437

Kwiatkowski, L., Torres, O., Bopp, L., Aumont, O., Chamberlain, M., Christian, J. R., et al. (2020). Twenty-first century ocean warming, acidification, deoxygenation, and upper-ocean nutrient and primary production decline from CMIP6 model projections. Biogeosciences, 17(13), 3439–3470. https://doi.org/10.5194/bg-17-3439-2020

Laurent, A., Fennel, K., & Kuhn, A. (2021). An observation-based evaluation and ranking of historical Earth system model simulations in the northwest North Atlantic Ocean. Biogeosciences, 18(5), 1803–1822. https://doi.org/10.5194/bg-18-1803-2021

Lillibridge, J. L., & Mariano, A. J. (2013). A statistical analysis of Gulf Stream variability from 18+ years of altimetry data. Deep Sea Research Part II: Topical Studies in Oceanography, 85, 127–146. https://doi.org/10.1016/j.dsr2.2012.07.034

Loder, J., Petrie, B., & Gawarkiewicz, G. (1998). The Coastal Ocean Off Northeastern North America: a large-scale view. In A. R. Robinson & K. H. Brink (Eds.), The global coastal ocean: regional studies and syntheses. New York: Wiley & Sons.

Lotze, H. K., Mellon, S., Coyne, J., Betts, M., Burchell, M., Fennel, K., et al. (2022). Long-term ocean and resource dynamics in a hotspot of climate change. FACETS, 7, 1142–1184. https://doi.org/10.1139/facets-2021-0197

Mertz, G., Narayanan, S., & Helbig, J. (1993). The freshwater transport of the labrador current. Atmosphere-Ocean, 31(2), 281–295. https://doi.org/10.1080/07055900.1993.9649472

Mills, K., Pershing, A., Brown, C., Chen, Y., Chiang, F.-S., Holland, D., et al. (2013). Fisheries Management in a Changing Climate: Lessons From the 2012 Ocean Heat Wave in the Northwest Atlantic. Oceanography, 26(2). https://doi.org/10.5670/oceanog.2013.27

Moreno-Chamarro, E., Caron, L.-P., Ortega, P., Tomas, S. L., & Roberts, M. J. (2021). Can we trust CMIP5/6 future projections of European winter precipitation? Environmental Research Letters, 16(5), 054063. https://doi.org/10.1088/1748-9326/abf28a

Moss, R. H., Edmonds, J. A., Hibbard, K. A., Manning, M. R., Rose, S. K., van Vuuren, D. P., et al. (2010). The next generation of scenarios for climate change research and assessment. Nature, 463(7282), 747–756. https://doi.org/10.1038/nature08823

Nye, J., Link, J., Hare, J., & Overholtz, W. (2009). Changing spatial distribution of fish stocks in relation to climate and population size on the Northeast United States continental shelf. Marine Ecology Progress Series, 393, 111–129. https://doi.org/10.3354/meps08220

Pershing, A. J., Alexander, M. A., Hernandez, C. M., Kerr, L. A., Le Bris, A., Mills, K. E., et al. (2015). Slow adaptation in the face of rapid warming leads to collapse of the Gulf of Maine cod fishery. Science, 350(6262), 809–812. https://doi.org/10.1126/science.aac9819

Peterson, I., Greenan, B., Gilbert, D., & Hebert, D. (2017). Variability and wind forcing of ocean temperature and thermal fronts in the S lope W ater region of the N orthwest A tlantic. Journal of Geophysical Research: Oceans, 122(9), 7325–7343. https://doi.org/10.1002/2017JC012788

Petrie, B., & Yeats, P. (2000). Annual and interannual variability of nutrients and their estimated fluxes in the scotian shelf - gulf of maine region. Canadian Journal of Fisheries and Aquatic Sciences, 57(12), 2536–2546.

Pozo Buil, M., Jacox, M. G., Fiechter, J., Alexander, M. A., Bograd, S. J., Curchitser, E. N., et al. (2021). A Dynamically Downscaled Ensemble of Future Projections for the California Current System. Frontiers in Marine Science, 8, 612874. https://doi.org/10.3389/fmars.2021.612874

Preisendorfer, R. (1988). Principal Component Analysis in Meteorology and Oceanography. Elsevier Science.

Rutherford, K., & Fennel, K. (2018). Diagnosing transit times on the northwestern North Atlantic continental shelf. Ocean Science, 14(5), 1207–1221. https://doi.org/10.5194/os-14-1207-2018

Rutherford, K., & Fennel, K. (2022). Elucidating Coastal Ocean Carbon Transport Processes: A Novel Approach Applied to the Northwest North Atlantic Shelf. Geophysical Research Letters, 49(6). https://doi.org/10.1029/2021GL097614

Rutherford, K., Fennel, K., Atamanchuk, D., Wallace, D., & Thomas, H. (2021). A modelling study of temporal and spatial pCO2 variability on the biologically active and temperature-dominated Scotian Shelf. Biogeosciences, 18(23), 6271–6286. https://doi.org/10.5194/bg-18-6271-2021

Rutherford, K., Fennel, K., Garcia Suarez, L., John, J. G., & Brickman, D. (2023). Uncertainty in the evolution of northwest North Atlantic circulation leads to diverging biogeochemical projections. EGUsphere [preprint], https://doi.org/10.5194/egusphere-2023-987, 2023

Saba, V. S., Griffies, S. M., Anderson, W. G., Winton, M., Alexander, M. A., Delworth, T. L., et al. (2016). Enhanced warming of the Northwest Atlantic Ocean under climate change. Journal of Geophysical Research: Oceans, 121(1), 118–132. https://doi.org/10.1002/2015JC011346

776 Seidov, D., Mishonov, A., Reagan, J., & Parsons, R. (2019). Resilience of the Gulf Stream path
777 on decadal and longer timescales. Scientific Reports, 9(1), 11549.
778 https://doi.org/10.1038/s41598-019-48011-9

779 Shin, S.-I., & Alexander, M. A. (2020). Dynamical Downscaling of Future Hydrographic
780 Changes over the Northwest Atlantic Ocean. Journal of Climate, 33(7), 2871–2890.
781 https://doi.org/10.1175/JCLI-D-19-0483.1

782 Simpson, J. (1981). The shelf-sea fronts: implications of their existence and behaviour.
783 Philosophical Transactions of the Royal Society of London. Series A, Mathematical and
784 Physical Sciences, 302(1472), 531–546. https://doi.org/10.1098/rsta.1981.0181

785 Stock, C. A., Alexander, M. A., Bond, N. A., Brander, K. M., Cheung, W. W. L., Curchitser, E.
786 N., et al. (2011). On the use of IPCC-class models to assess the impact of climate on
787 Living Marine Resources. Progress in Oceanography, 88(1–4), 1–27.
788 https://doi.org/10.1016/j.pocean.2010.09.001

789 Stommel, H. M., & Leetmaa, A. (1972). Circulation on the continental shelf. Proceedings of the
790 National Academy of Sciences of the United States of America, 69 11, 3380–4.

791 Taylor, K. E., Stouffer, R. J., & Meehl, G. A. (2012). An Overview of CMIP5 and the
792 Experiment Design. Bulletin of the American Meteorological Society, 93(4), 485–498.
793 https://doi.org/10.1175/BAMS-D-11-00094.1

794 Urrego-Blanco, J., & Sheng, J. (2012). Interannual Variability of the Circulation over the Eastern
795 Canadian Shelf. Atmosphere-Ocean, 50(3), 277–300.
796 https://doi.org/10.1080/07055900.2012.680430

797 Zhang, J., Weijer, W., Steele, M., Cheng, W., Verma, T., & Veneziani, M. (2021). Labrador Sea
798 freshening linked to Beaufort Gyre freshwater release. Nature Communications, 12(1),
799 1229. https://doi.org/10.1038/s41467-021-21470-3

800 Zisserson, B., & Cook, A. (2017). Impact of bottom water temperature change on the
801 southernmost snow crab fishery in the Atlantic Ocean. Fisheries Research, 195, 12–18.
802 https://doi.org/10.1016/j.fishres.2017.06.009